Equation-of-state measurements of polyimide at pressures up to 5.8 TPa using low-density foam with laser-driven shock waves

K. Takamatsu,[1,2] N. Ozaki,[1,2] K. A. Tanaka,[1,2] T. Ono,[1,2] K. Nagai,[1] M. Nakai,[1] T. Watari,[1] A. Sunahara,[1] M. Nakano,[2] T. Kataoka,[2] H. Takenaka,[3] M. Yoshida,[4] K. Kondo,[5] and T. Yamanaka[1]

[1]*Institute of Laser Engineering, Osaka University, Osaka 565-0871, Japan*

[2]*Faculty of Engineering, Osaka University, Osaka 565-0871, Japan*

[3]*NTT Advanced Technology Corporation, Tokyo 180-8585, Japan*

[4]*National Institute of Advanced Industrial Science and Technology (AIST), Ibaraki 305-8565, Japan*

[5]*Materials and Structures Laboratory (MSL), Tokyo Institute of Technology, Kanagawa 226-8503, Japan*

(Received 28 May 2002; revised manuscript received 25 February 2003; published 23 May 2003)

The laser-driven equation-of-state (EOS) experiments for polyimide are presented. The experiments were performed with emission measurements from the rear sides of shocked targets at up to a laser intensity of 10^{14} W/cm^2 or higher with 351 nm wavelength and 2.5 ns duration. Polyimide Hugoniot data were obtained up to 0.6 TPa with good accuracy. Applying low-density foam ablator to the EOS unknown material, we also obtained the data at a highest pressure of 5.8 TPa in the nonmetal materials. Those data were in agreement with the theoretical curves.

DOI: 10.1103/PhysRevE.67.056406 PACS number(s): 52.50.Jm, 64.30.+t, 52.35.Tc, 62.50.+p

I. INTRODUCTION

The study on the equation-of-state (EOS) of matters in extremely high-pressure conditions is of great interest in several fields of modern physics [1]. In particular, the inertial fusion energy (IFE) researches, the shock structure, the compression efficiency, and the gain in the fusion capsules critically depend on the EOS of the fuel capsule materials.

In the studies, the typical target-shell material of direct-drive experiments is low-density hydrocarbon polymers such as polystyrene. These materials meet the immediate requirements for the IFE target shell, i.e., low density, smooth outer and inner surfaces, sphericity, and concentricity. The future IFE experiments, especially those conducted at cryogenic temperatures, would be more feasible if the targets possessed additional properties such as high tensile strength, large elastic module, great room-temperature permeability, large radiation resistance, high thermal conductivity, low electrical conductivity, and large opacity at a laser wavelength of 351 nm. These properties allow the target shell to be filled more rapidly with an equimolar ratio of deuterium and tritium (DT), to be cooled faster to the DT triple point (19.8 K), to survive higher temperature gradients in a cryostat, and to resist the damaging effects of β-decay from tritium. These properties allow also thin wall shells to contain the DT fuel.

Polyimide (PI) is a good polymeric material with a potential of meeting these additional requirements. PI shells were first suggested for the National Ignition Facility (NIF) [2]. Recently, the high-quality millimeter-sized PI shells have been fabricated by vapor deposition polymerization [3] and by removing nonvolatile solvent [4]. PI is also used as the ablator of multilayered flyer that we developed to generate high pressures without the preheat problem by laser-plasma interactions [5,6]. As there is no Hugoniot data for PI in TPa pressure region, the shock compressed state should be known in order to design experiments using PI.

Powerful laser-induced shocks have extended the capability of high-pressure EOS studies, providing TPa (10 Mbars) pressures [7], even for low-Z plastic materials [8,9] for which only theoretical model and calculation were available. The planarity and temporal steadiness of the laser shock are essential factors to obtain the accurate EOS data. The recent experiments proved the possibility to create spatially uniform shocks in solids by using a direct drive with optically smoothed laser beams [10] and by using thermal x rays from laser-heated cavity to generate shocks (indirect drive) [11]. In addition, our laser flyer method produced a quite flat shock [6].

Accurate measurements can be performed if high-quality shock waves are generated. Generally, the EOS experiments measure two independent variables under shock compression simultaneously and calculate the rest from the Rankine-Hugoniot relations [12]. The most popular method for the determination of EOS points is self-emission measurement with using double-step targets. This method utilizes the impedance-mismatching (IM) technique [12], measuring the two shock velocities simultaneously in two materials: a standard and a sample to be investigated. This makes it possible to determine one Hugoniot point of the sample material based on the EOS of the reference material. In recent experiment, the absolute experiments independently measuring two parameters were carried out with x-ray radiography [9,13]. However, such absolute experiments require very high-power laser systems with long pulse duration to generate a main shock loading and a strong backlighter x-ray pulse. It is indicated that the arrangement between the target and the diagnostic apparatus is very difficult because the tilt of the target strongly affects the measured compressibility [14].

In this paper, presented are the direct laser-driven experiments of PI EOS. The self-emission measurements are described based on the impedance-mismatching scheme using double-step targets. Data are shown up to a highest pressure in the nonmetal materials, which is obtained by a low-density foam ablator working as a pressure amplifier.

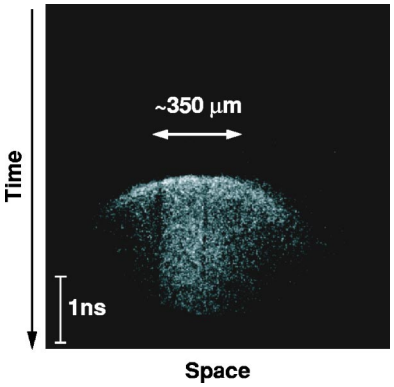

FIG. 1. Typical streaked image of the self-emission at the target rear surface. Time proceeds from the top to the bottom.

II. EXPERIMENTS

The experiment was performed using the ''HIPER'' laser facility, a new irradiation system of the GEKKO XII (GXII) laser system at the Institute of Laser Engineering (ILE), Osaka University [15]. The HIPER was built to investigate the hydrodynamic physics at 10^{14} W/cm^2 laser intensity or higher. Twelve beams of the GXII are bundled in a $F/3$ cone angle and can provide high intensity and uniform irradiation conditions. We used nine beams smoothed by spectral dispersion (SSD) and by the kinoform phase plates at 351 nm (third harmonics of the GXII: 3ω). The temporal behavior of the laser pulse was approximately of square shape with a full width at half maximum time of 2.5 ns and a rise and a fall time of 100 ps. The laser beams were focused onto a target with a 600 μm diameter.

The IM scheme was applied on double-step targets to obtain the two different shock speeds. When a shock wave propagates in a target, the shock breakout at the target's rear surface emits a thermal radiation depending on the shock temperature. The emission was measured with a visible streak camera. The self-emission signals were collected by an $F/2.8$ of relay lens and the image was relayed on the slit of the streak camera by a microscopic objective ($M=5$) and an achromatic lens with a focal length $f=400$ mm. The image of the vertically arranged step target edge was rotated by 90° by a dove prism on the streak slit. Taking into account the use of band-cut filters of the harmonics of the GXII (2ω and 3ω), the detectable wavelength of the diagnostics system was between 400 and 800 nm excluding the spectral region close to 2ω. The temporal resolution was better than 25 ps, and the spatial resolution was 7 μm on the target in this experiment.

Figure 1 shows a typical example of streaked images of the emission at planar target rear surface. The size of the central sufficiently planar region of generated shocks is about 350 μm in diameter.

III. TARGETS

In our IM experiments, we used two types of double-step targets with the structures shown in Fig. 2. The first one, shown in Fig. 2(a), is made of an Al base layer and two

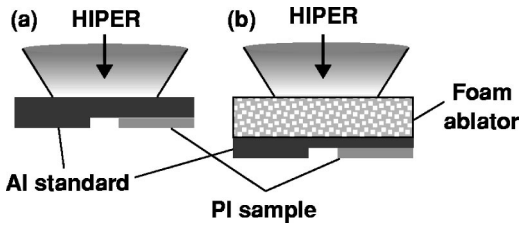

FIG. 2. (a) Typical double-step target and (b) target with a foam ablator. The foam and PI surfaces are overcoated with a thin Al layer.

steps: Al and PI as samples. This PI is a soluble and highly transparent polyimide that is synthesized by the reaction of 2,2′-bis(trifluoromethyl)-4,4′-diaminobiphenyl with 2,2′-bis(3,4′-dicarboxyphenyl)hexafluoropropane dianhydride. We optimize both the base and the step thicknesses under our laser condition to keep steady shock waves in the target, using the numerical code MY1DL based on a one-dimensional hydrodynamic Lagrangian code [16]. We use the Al EOS data in the simulation from the SESAME table [17]. Since there is no data of PI (the initial density $\rho_0^{\mathrm{PI}}=1.50$ g/cm^3) in the SESAME, we substitute a mixed material of two plastics, teflon ($\rho=2.15$ g/cm^3) and parylene-d ($\rho=1.42$ g/cm^3), to have the PI density. The optimized thicknesses were 40 μm of Al base, 20 μm of Al step, and 7–9 μm of PI step. In Fig. 2(b), a plastic [poly(4-methyl-1-pentene), PMP] foam layer is placed on the laser side of the target. This target is for acquiring pressures higher than those produced in simple structure targets. There is also no EOS data for the low-density foam ($\rho\approx0.1$ g/cm^3) in the SESAME. A simple model treating rarefaction wave [18] was used to determine the thicknesses of the foam, Al and PI layers. The foam layer ($\rho\approx0.1$ g/cm^3) was 150 μm thickness, the Al base and step thicknesses are 9–10 μm, and the PI step thickness is 7–9 μm, respectively.

In order to make the experimental errors as small as possible, the targets should be precisely made and should be well characterized. Stepped targets have been often produced with an electron gun deposition. This fabrication technique may result in the density lower than the bulk density and its strength weaker than the bulk. We developed a adhesion technique, using single molecular membrane coating [19], and applied it to the target preparation. The adhesion force was sufficient in not only Al-Al but also in Al-PI interfaces. The thickness of the adhesion layer was less than 1% (≈several hundreds angstroms) of the step thickness. The free surface of PI was overcoated with a 1000-Å Al layer in order to observe the timing of the shock breakout. The low-density plastics (PMP) foam was produced on the Al foil using a freeze drying method. Figure 3 shows scanning electron microscope (SEM) images of the foam surface and cross section, we can see holes (cell size of ~3 μm) located in the whole surface of the foam. The density of this foam is 0.1 g/cm^3. The foam surface was coated with a 500-Å Al layer that eliminated a laser shine through into the foam at the start of laser pulse.

IV. EXPERIMENTAL RESULTS AND DISCUSSION

Figure 4 shows a typical example of streaked images of the rear emission from double-step target. In this shot, the

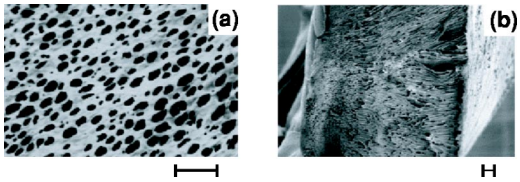

FIG. 3. SEM images of the plastics foam (a) surface and (b) cross section. Scales denote 10 μm. The density of the foam is 0.1 g/cm^3, and the thickness is 150 μm. The cell size is approximately 3 μm.

target was irradiated by four beams whose laser intensity was 3.1×10^{13} W/cm^2.

At this laser irradiance, preheating by suprathermal electrons is negligible since the laser intensity is well below the threshold for any nonlinear parametric instability. Our laser wavelength and beam smoothing by the SSD should be effective to reduce any parametric instabilities. In these experimental conditions, preheating is mainly due to the x rays from the critical density plasma [20]. In our experiments, no significant emission was detected prior to the shock arrival due to preheat. Additionally, we measured reflected-probe light from the target rear surface by using a velocity interferometer system up to 6.6×10^{13} W/cm^2 laser intensity. The reduction of reflectivity was not observed before shock arrival; the reflectivity decreased rapidly at the emergence of shock. Our highest pressure data were obtained using a plastic foam ablator. It was measured that the foam ablator effectively minimized the radiation preheating [20,21]. Measuring x-ray intensity at a laser-irradiated surface with x-ray pinhole (time integrated) and x-ray framing (time resolved) cameras in all shots, we confirmed that the x-ray intensity in case of the foam was one order of magnitude lower than in the case of Al.

In Fig. 4, the time interval Δt^{Al} corresponds to the transit time of the shock wave through the Al step, and Δt^{PI} is that of the PI step. The thicknesses of these steps were accurately measured by a laser focusing height meter with a resolution of 0.01 μm. In this data, Δt^{Al} and Δt^{PI} were 887.4 ± 5.1 ps and 306.0 ± 5.1 ps, and the thicknesses of Al and PI steps were 19.42 ± 0.10 μm and 7.99 ± 0.05 μm, respectively.

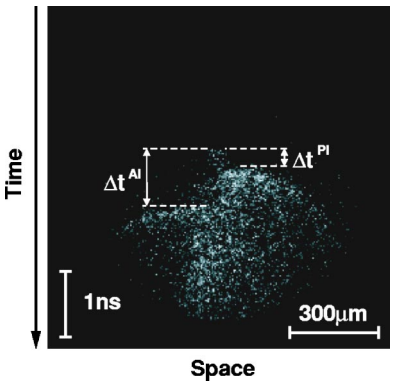

FIG. 4. Typical streaked image of emission measurements with double-step target. Time intervals Δt^{Al} and Δt^{PI} indicate the transit time of the shock wave through the Al and PI steps, respectively.

Therefore the shock velocities D of Al and PI were 21.9 km/s with 1.0% error and 26.1 km/s with 2.4%. The Al initial density ρ_0^{Al} was 2.71 g/cm^3 and the PI initial density ρ_0^{PI} was 1.50 g/cm^3 with errors of less than 1%.

Al Hugoniot data had been accurately investigated over a wide range of pressures. As known well, both theory and many experiments in Al suggest linear $D-U$ (shock and particle velocity) relationships. Here, we used a linear relation suggested by Mitchell and Nellis [22]:

$$D=(5.386\pm0.047)+(1.339\pm0.021)U. \tag{1}$$

Then the particle velocity U^{Al} of Al and the pressure P^{Al} of Al corresponding to the $D^{\mathrm{Al}}=21.9$ km/s, were 12.3 km/s and 730 GPa, respectively. U^{Al} has 1.9% error, and P^{Al} has 2.1% error.

U^{Al} and P^{Al} were calculated by the IM method. In this case, since PI has a lower shock impedance than Al, an unloading wave is reflected in Al when the shock goes through the interface between the two materials. The propagation of this wave is governed by an isentropic flow [12], originating from the point $(P^{\mathrm{Al}},U^{\mathrm{Al}})$ which is given by

$$U(P)=U^{\mathrm{Al}}-\int_{P^{\mathrm{Al}}}^{P}\left(-\frac{\partial V}{\partial P}\right)_S^{1/2}dP, \tag{2}$$

where V is volume of Al.

The intersection of this release is given by

$$P^{\mathrm{PI}}=\rho_0^{\mathrm{PI}}D^{\mathrm{PI}}U^{\mathrm{PI}} \tag{3}$$

in the (P,U) plane with the conservation of momentum. Equations (2) and (3) give the particle velocity and pressure of the shock in PI. U^{PI} and P^{PI} were 15.3 km/s and 589 GPa, respectively. The error of U^{PI} was 1.9% and that of P^{PI} was 3.1%.

Four PI Hugoniot data points have been first obtained in TPa region and are plotted in Fig. 5. The open diamonds indicate present work. The solid and open circles are our previous data using the lasers and explosives, respectively [23]. The solid curve is the Hugoniot of PI predicted by mixing two plastics in the SESAME. The dashed curve is Hugoniot calculated from QEOS [24]. The errors of these three data in the sub-TPa pressure range were 1.9–2.4 % at particle velocity and 3.1–4.5% at pressure. These were in good agreement with the theoretical extrapolations.

The data of 5.8 TPa, as a result of utilizing pressure-amplification effect by the low-density foam ablator, is one of the highest pressures in the nonmetal materials. The generated pressure in Al was 7.4 TPa. The ablation pressure was estimated as $\approx$2.6 TPa by numerical simulation at same laser condition in the shot. The pressure amplification effect can be evaluated as about 2.8. The fact is very consistent with an expectation in our foam density, according to Batani *et al.* [18]. Taking into account the errors for U (58.25 km/s with 12.2%) and P (5.8 TPa with 19.0%), the result supports the theoretical curves. In such extremely high pressure, Δt became very small; the errors arising from Δt increased. The errors may be reduced to be less than 6% in U and less than

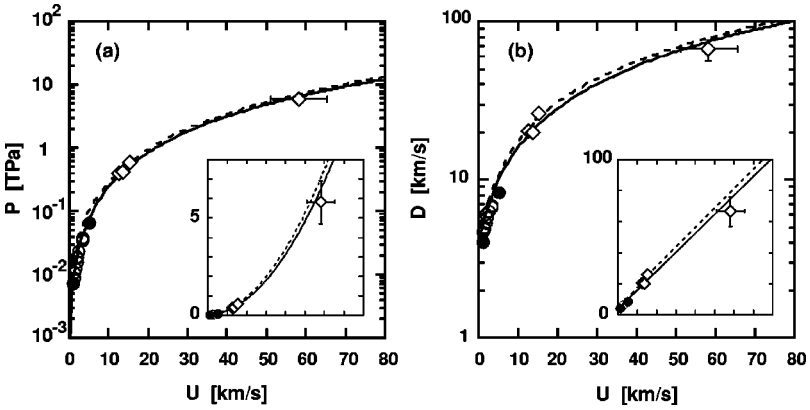

FIG. 5. PI Hugoniot data presented as (a) P vs U and (b) D vs U. These are single logarithmic plots for showing the data difference (insets are conventional representations; it is difficult to distinguish low-pressure data). Present experiments (open diamonds) and past data by lasers (solid circles) and by explosives (open circles) [23] are compared to PI Hugoniot data predicted from the SESAME tabular EOS (solid curve) and from the QEOS [24] (dashed curve).

10% in P by improving the two points. The sweep speed of a streak camera can be twice as fast and the thickness error of the target step should be 3% than 5–6 % in the experiment.

The highest pressure data is a bit lower than the theoretical curves, and indicates a quite high compressibility of more than 7. However, we need to be careful about this compressibility because the maximum compression by an single shock is, as an indication, the fourfold of the initial density. Here, this extreme compression may result from several possibilities. First, the thermodynamic equilibrium in the shocked target might be insufficient. The shock temporal steadiness is one of the very important things for Hugoniot measurements. The duration of the highest pressure with foam is shorter than without foam because rarefaction wave catches up with the shock front immediately. Therefore, the target shown in Fig. 2(b) is made with thin Al foils. The generated condition could be in a shock acceleration phase and may not be sufficiently in equilibrium during such short transit time of shock.

The second possibility is relevant to the error of standard EOS. In such a extreme pressure, Eq. (1) may not be the best expression of the linear relation between D and U, although the equation is very good fit to the experimental Hugoniot data in sub-TPa region [22]. When the total pressure in Al is divided into cold (zero Kelvin), ion-thermal, and electron-thermal contributions, the cold and ion components are dominant in the sub-TPa pressures on the Hugoniot, while the ion and electron contributions are to increase in the TPa regime [25]. We may need to utilize a different reliable statistical curve in the ultrahigh pressure region. Moreover, in this region the isentrope is not confirmed experimentally. It is surely worthy to verify the isentrope at multi-TPa pressures in further experiments to decrease the error.

Preheating problem, of course, influences the Hugoniot data. However, if there is a problem, generally the compressibility does not increase. The radiation preheating causes the increase in the temperature and hence in the shock velocity of the sample, and the increase in the shock propagating distance due to free surface expansion. Finally, the competition between these factors allows shock-breakout measurements to be insensitive to the radiation preheating. Preheating is not responsible in any way to the observed high compression of PI.

V. CONCLUSIONS

In conclusion, EOS experiments have been performed with laser-driven shock waves using the HIPER laser system. Self-emission measurement based on the IM method was carried out. Hugoniot data of PI which is useful to the IFE and our laser flyer studies were measured. In the target fabrication, a gluing technique using single molecular membrane coating was adopted in the adhesion of Al-Al and Al-PI. The principal Hugoniot data of PI were obtained up to 0.6TPa with error less than 3%. The low-density foam ablator for pressure amplification was applied measure the EOS of the unknown material (PI). The Hugoniot data at a highest pressure of 5.8 TPa were obtained utilizing the amplification effect.

ACKNOWLEDGMENTS

The authors gratefully acknowledge the valuable support for the experiment by the GXII technical crews and scientists at the ILE. In particular, the author would like to thank H. Azechi, H. Shiraga, K. Shigemori, and K. Nishihara for fruitful discussions, K. Suzuki, S. Urushihara, H. Asahara, and N. Morio for operating the GXII, O. Maegawa, K. Shimada, T. Kuwamoto, and Y. Hori for diagnostic support, and Y. Kimura, T. Norimatsu and his group for target fabrications. The authors would like to thank K. Okada, K. Wakabayashi (AIST), and H. Nagao (MSL) for fruitful discussions and useful comments. K.T. and N.O. would like to thank M. Nishikino and S. Fujioka for valuable experimental support, and H. Nishimura for preparing diagnostic systems. This work was performed under the auspices of the Japan Science and Technology Corporation (JST) by Osaka University under Contract No. A2-12308020.

[1] W.J. Nellis *et al.*, Science (Washington, DC, U.S.) **269**, 1249 (1995); D. Saumon *et al.*, Astrophys. J., Suppl. Ser. **99**, 713 (1995); W.J. Nellis, Planet. Space Sci. **48**, 671 (2000); C.S. Yoo *et al.*, Phys. Rev. Lett. **70**, 3931 (1993); S.W. Haan *et al.*, Phys. Plasmas **2**, 2480 (1995); J.D. Lindl, *ibid.* **2**, 3933 (1995).
[2] J.J. Sanchez and S.A. Letts, Fusion Technol. **31**, 491 (1997); T.R. Dittrich *et al.*, Phys. Plasmas **6**, 2164 (1999).
[3] F.-Y. Tsai *et al.*, J. Phys. D **34**, 3011 (2001).
[4] K. Nagai *et al.*, Macromol. Rapid Commun. **22**, 1344 (2001).
[5] K.A. Tanaka *et al.*, Phys. Plasmas **7**, 676 (2000); T. Kadono *et al.*, J. Appl. Phys. **88**, 2943 (2000).
[6] N. Ozaki *et al.*, J. Appl. Phys. **89**, 2571 (2001).
[7] M. Koenig *et al.*, Phys. Rev. Lett. **74**, 2260 (1995); A.M. Evans *et al.*, Laser Part. Beams **14**, 113 (1996); A. Benuzzi *et al.*, Phys. Rev. E **54**, 2162 (1996); D. Batani *et al.*, Phys. Rev. B **61**, 9287 (2000); D. Batani *et al.*, Phys. Rev. Lett. **88**, 235502 (2002).
[8] M. Koenig *et al.*, Appl. Phys. Lett. **72**, 1033 (1998).
[9] R. Cauble *et al.*, Phys. Rev. Lett. **80**, 1248 (1998).
[10] M. Koenig *et al.*, Phys. Rev. E **50**, R3314 (1994).
[11] Th Löwer *et al.*, Phys. Rev. Lett. **72**, 3186 (1994).
[12] Ya.B. Zeldovich and Yu.P. Raizer, *Physics of Shock Waves and High Temperature Hydrodynamic Phenomena* (Academic, New York, 1967).
[13] L.B. Da Silva *et al.*, Phys. Rev. Lett. **78**, 483 (1997); G.W. Collins *et al.*, Science **281**, 1178 (1998).
[14] W.J. Nellis, Phys. Rev. Lett. **89**, 165502 (2002).
[15] M. Nakatsuka, *Annual Progress Report of Institute of Laser Engineering* (Osaka University Press, Osaka, 2001), p. 1.
[16] M. Yoshida, CETR Report No. C-06-86, 1986 (unpulished).
[17] SESAME: the LANL equation of state database, LA-UR-92-3407, Los Alamos National Laboratory (1992). Copies may be ordered from the National Technical Information Service, Springfield, VA 22161.
[18] D. Batani *et al.*, Phys. Rev. E **63**, 046410 (2001).
[19] K. Nagai *et al.*, Jpn. J. Appl. Phys., Part 2 **41**, L1184 (2002).
[20] A. Benuzzi *et al.*, Phys. Plasmas **5**, 1 (1998).
[21] H. Pépin *et al.*, Phys. Fluids **28**, 3393 (1985).
[22] A.C. Mitchell and J.W. Nellis, J. Appl. Phys. **52**, 3363 (1981).
[23] N. Ozaki *et al.*, Phys. Plasmas (to be published).
[24] R.M. More *et al.*, Phys. Fluids **31**, 3059 (1988).
[25] A.C. Mitchell *et al.*, J. Appl. Phys. **69**, 2981 (1991).